11th International Symposium on Turbulence and Shear Flow Phenomena (TSFP11)
Southampton, UK, July 30 to August 2, 2019

ON THE ONSET OF TRANSITION IN 90°-BEND PIPE FLOW

Valerio Lupi
Linné FLOW Centre, KTH Mechanics
KTH Royal Institute of Technology
SE-100 44 Stockholm, Sweden
lupi@kth.se

Jacopo Canton
Computational Science and Engineering
Laboratory, ETH Zurich
CH-8092 Zurich, Switzerland
jcanton@ethz.ch

Philipp Schlatter
Linné FLOW Centre, KTH Mechanics
KTH Royal Institute of Technology
SE-100 44 Stockholm, Sweden
pschlatt@mech.kth.se

ABSTRACT

The present work deals with the global stability analysis of the flow in a 90°-bend pipe with curvature $\delta = R/R_c = 0.3$, being R the radius of the cross-section of the pipe and R_c the radius of curvature at the pipe centreline. Direct numerical simulations (DNS) for values of the bulk Reynolds number $Re_b = \frac{U_b D}{\nu}$ between 2000 and 3000 are performed. The bulk Reynolds number is based on the bulk velocity U_b, the pipe diameter D, and the kinematic viscosity ν. It is found that the flow is steady for $Re_b \leq 2500$, and two pairs of symmetric, counter-rotating vortices are observed in the section of the pipe downstream of the bend. Moreover, two recirculation regions are present inside the bend, one on the outer wall and the other on the inner one. For $Re_b \geq 2550$, the flow becomes periodic, oscillating with a fundamental non-dimensional frequency $St = fD/U_b = 0.23$. A global stability analysis reveals a pair of complex conjugate eigenvalues with positive real part. The velocity components of the unstable direct and adjoint eigenmodes are investigated, and it is observed that a large spatial separation occurs because of the non-normality of the linearised Navier–Stokes operator. Thus, an analysis of the structural sensitivity of the unstable eigenmode to spatially localised feedbacks is performed, in order to identify the core of the instability, the so-called *wavemaker*. It is found that the region located 15° downstream of the bend inlet, on the outer wall, is where the instability originates. Since flow separation is observed in this region, it is concluded that the instability is linked with the strong shear by the backflow phenomena.

INTRODUCTION

In previous works on bent pipes, a secondary motion in the form of two symmetric, counter-rotating vortices, known as Dean vortices, was observed. Indeed, as shown by Dean (1927) in the limit of small curvatures, the secondary motion is established in order to balance the centrifugal force, since the cross-stream pressure gradient alone cannot counteract it. This secondary flow enhances, *e.g.*, heat transfer and mixing. Moreover, due to the Dean vortices, the pressure drop has a lower magnitude near the outer side of the bend compared to the inner side, differently from the straight pipe case, as outlined in Berger *et al.* (1983).

The understanding of the flow in bent pipes is crucial since they are used in several industrial applications, *e.g.* to transport gases and fluids, in the exhaust system of internal combustion engines, and in cooling systems of nuclear reactors. Indeed, in the last decades, increasing attention has been paid to the study of this kind of flow in order to improve the design of pumping systems and heat exchangers, as well as the accuracy of measurements on pipelines (Vashisth *et al.*, 2008). In addition, the secondary motion may induce vibrations (Yamano *et al.*, 2011), and the consequent mechanical fatigue, and has a fundamental role also in the mechanism of thermal fatigue (Tunstall *et al.*, 2016). The understanding of this flow is important also from a biological point of view. Indeed, the investigation of the maxima and minima of the wall shear stress in blood vessels provides information on the formation of atheromatous plaques (Berger *et al.*, 1983).

Recently, Kühnen *et al.* (2014, 2015), by means of experimental investigations, provided a detailed overview of the sequence of bifurcations that lead to transition to turbulence in toroidal pipe flows and observed that subcritical transition occurs for values of the curvature $\delta \leq 0.028$. In a numerical work by Canton *et al.* (2016), it was found that the flow in a torus is linearly unstable for all the values of the curvature greater than $2 \cdot 10^{-3}$, and it was observed that the instability occurs as a Hopf bifurcation leading to a periodic regime. Numerical simulations also showed the presence of two symmetric, counter-rotating vortices for any Reynolds number and any non-zero curvature, a result proven analytically in a later work (Canton *et al.*, 2017). Furthermore, it was pointed out that the Dean number alone cannot fully characterise the flow behaviour. Indeed, Canton *et al.* (2017) showed that the flow in curved pipes depends separately on the Reynolds number and on the curvature. Rinaldi *et al.* (2019) observed subcritical transition in curved pipes with $\delta = 0.01$ for $2950 \lessapprox Re_b \lessapprox 3100$. It occurs as the intermittent coexistence of laminar and turbulent flow. However, the front dividing the two was found to be not as

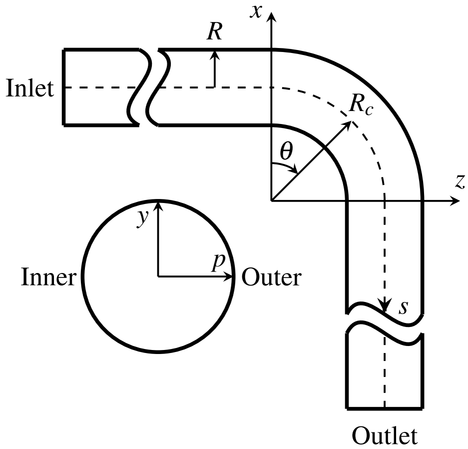

Figure 1: Reference system used in the current work, together with the Cartesian coordinates. R is the radius of the pipe, R_c the radius of curvature, θ is the angular distance from the bend inlet.

strong as in the straight pipe case. Furthermore, in a recent work by Canton *et al.* (2019), it was found that, in a narrow region of the parameter space (δ, Re_b), two different transition scenarios are possible at the same time, depending on the initial condition.

The aforementioned works studied the stability of the flow in toroidal pipes; however, to the best of the authors' knowledge, in the literature, there are no studies on the stability properties of the flow in a 90°-bend.

COMPUTATIONAL SETUP

The computational domain consists of two straight sections, located up and downstream of the bend and $10D$ long each, and a 90°-bend, with radius of curvature equal to three times the radius of the pipe. The domain is discretised with hexahedral spectral elements where Lagrangian bases with polynomial order $N = 7$, built on tensor-product Gauss–Lobatto–Legendre (GLL) nodes, are used. The Navier–Stokes equations are expressed in Cartesian coordinates and direct numerical simulations (DNS) are performed using the spectral-element code `nek5000` (Fischer *et al.*, 2008). In the post-processing phase, a local reference system $\{p, y, s\}$ is introduced, as shown in Figure 1. The coordinate y is the same of the Cartesian coordinate system, s is the streamwise coordinate along the pipe centreline with origin at the bend exit, and p, referred to as spanwise coordinate, forms a right-turning triad with y and s.

INSTANTANEOUS FLOW FIELDS

The flow is found to be steady for $Re_b \leq 2500$, with fairly complex flow structures, as shown in Figure 2. For this flow case, a parabolic profile is specified at the inflow at a distance upstream of the bend. Then, two pairs of symmetric, counter-rotating vortices are observed downstream of the bend: two larger vortices, identified with the Dean vortices, are located at the centre of the pipe cross-section, whereas two smaller ones are close to the inner wall. As the distance downstream of the bend increases, the latter pair moves towards the centre of the pipe, at expenses of the Dean vortices. Thus, a so-called four vortex state can be seen in this spatially-developing configuration (Nandakumar & Masliyah, 1982); the fully developed flow in a torus, on the other hand, only features one pair of Dean vortices. Figure 3 shows two backflow regions inside the bend, one placed at the outer wall of the pipe, between $\theta = 0°$ and $\theta = 30°$, and a second one located on the inner bend, approximately 67.5° downstream of the bend inlet.

The lowest Reynolds number, among the investigated ones, for which the flow is found to be unsteady is equal to 2550. For this value of Re_b, a periodic regime is established. In particular, it is observed that the backflow regions exhibit an oscillatory behaviour, with a fundamental frequency corresponding to a Strouhal number $St = fD/U_b = 0.23$. The same frequency is measured in the oscillations of the streamwise velocity component, as shown in Figure 4. Note that the streamwise direction is always defined in the direction of the main flow, *i.e.* following the bend. It can be noted that the frequency content of higher harmonics increases with the streamwise distance. This indicates that the initial instability is likely of linear nature, and that nonlinear interactions become more and more important further downstream. Thus, a global stability analysis is performed next in order to investigate the origin of this periodic regime.

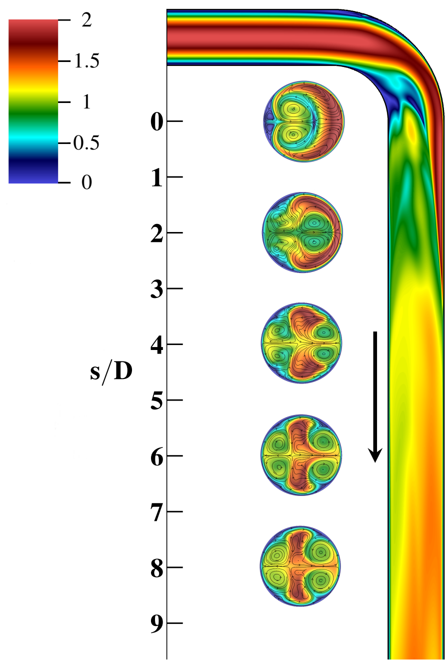

Figure 2: Pseudocolours of the velocity magnitude in the symmetry plane and on cross-sections along the pipe at $Re_b = 2500$. In-plane streamlines are shown on the cross-sections as well; their location is $s/D = 0, 2, 4, 6, 8$. The arrow indicates the flow direction. Only part of the inlet section is shown.

GLOBAL STABILITY ANALYSIS

The first step of the global stability analysis is to compute the base flow at $Re_b = 2550$, which is a steady equilibrium solution of the Navier–Stokes equations. Since this solution is unstable for the value of the Reynolds number considered, the `BoostConv` algorithm, developed by Citro

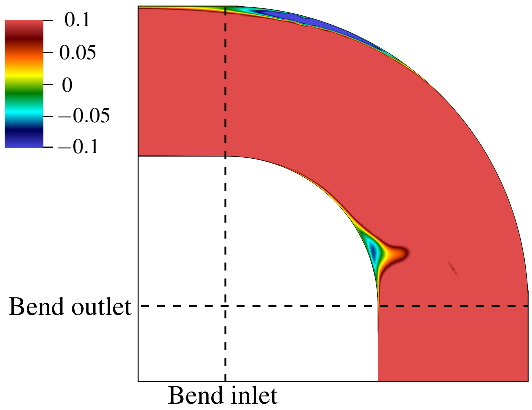

Figure 3: Pseudocolours of the streamwise velocity component inside the bend at $Re_b = 2500$. Green and blue areas indicate backflow regions.

et al. (2017), is employed in order to stabilise it. The algorithm is called every 50 time units of the non-linear solver, and a Krylov subspace of size 25 is used. It is assumed that the flow has reached the steady state when the Euclidean norm of the difference between the velocities computed at two consecutive iterations is less than 10^{-10}. The resulting base flow presents a morphology which resembles the steady flow at $Re_b = 2500$. This is expected because of the small difference in the Reynolds number.

Once the base flow is computed, the Navier–Stokes equations can be linearised around it in order to obtain the perturbation equations. Using the normal-mode hypothesis, the velocity and pressure fields are then expressed as

$$\begin{aligned} \boldsymbol{u}'(\boldsymbol{x},t) &= \hat{\boldsymbol{u}}(\boldsymbol{x})\, e^{\lambda t}, \quad \lambda \in \mathbb{C} \\ p'(\boldsymbol{x},t) &= \hat{p}(\boldsymbol{x})\, e^{\lambda t}, \quad \lambda \in \mathbb{C} \end{aligned} \tag{1}$$

where $\lambda = \sigma + i\omega$, being σ the growth rate and ω the frequency. In this way, the generalised eigenvalue problem can be recast in the form

$$\lambda M \hat{\boldsymbol{q}} = J \hat{\boldsymbol{q}} \tag{2}$$

where $\hat{\boldsymbol{q}} = \begin{pmatrix} \hat{\boldsymbol{u}} \\ \hat{p} \end{pmatrix}$. However, the explicit construction of the matrices M and J is too demanding in terms of storage and computational cost, and therefore a matrix-free method is used, as described in Bagheri *et al.* (2009). By exploiting the incompressibility constraint and the boundary conditions, it is possible to write the perturbation equations as an initial value problem (Schlatter *et al.*, 2011), such that the solution is

$$\boldsymbol{u}(\boldsymbol{x},t) = e^{Lt}\, \boldsymbol{u}_0(\boldsymbol{x}), \tag{3}$$

where e^{Lt} is a matrix exponential. It can be proven (Bagheri *et al.*, 2009) that the eigenvalues of e^{Lt} are related to those of L. Moreover, the explicit construction of the matrix exponential is not needed since its effect on a vector can be computed by time-marching the Navier–Stokes equations. Hence, using snapshots of the flow field separated by a constant time interval, a Krylov subspace is built and the eigenvalues are computed by means of the implicitly restarted Arnoldi method (IRAM) proposed by Sorensen (1992) and implemented in the software package `ARPACK` (Lehoucq *et al.*, 1998). This method avoids the storage of a large number of eigenvectors since it combines the Arnoldi factorization with the implicitly shifted QR scheme.

In the present work, we use the implementation of the Arnoldi algorithm in Nek5000 described by Peplinski *et al.* (2015). 20 eigenpairs are computed both for the direct and the adjoint problem, and the resulting spectra are shown in Figure 5. The spectrum of the adjoint problem is well in agreement with that of the direct one, apart from two stable eigenvalues that exhibit a relevant deviation. However, since the current analysis focuses mainly on the unstable part of the spectrum, the eigenvalues are well approximated for the purpose of this work. A pair of unstable complex conjugate eigenvalues is found, with a frequency $\omega = 1.4402$ corresponding to $St = 0.229$, which is in good agreement with the value $St = 0.23$ observed in DNS, being their relative difference lower than 1%. This result confirms that the flow undergoes a Hopf bifurcation between $Re_b = 2500$ and $Re_b = 2550$. A better estimate of the critical Reynolds number is provided by computing the eigenvalues at $Re_b = 2500$ and performing a linear interpolation between the values of the growth rate of the least stable mode in both the stable and unstable case. It is found that the critical Reynolds number is approximately 2529, hence much lower than the value $Re_{b,cr} \approx 3379$ computed by Canton *et al.* (2016) in the case of a toroidal pipe with the same curvature $\delta = 0.3$. This means that, albeit undergoing the same kind of bifurcation, bent pipes preceded and followed by straight sections exhibit different stability properties with respect to curved pipes, and therefore have to be studied separately. This result is perhaps not surprising given the complex spatially developing base flow, as shown in *e.g.* Figure 2.

The spatial structure of the unstable direct eigenmode is analysed: the mode is symmetric with respect to the spanwise direction, and the spanwise velocity component exhibits relevant amplitudes in the section downstream of the bend exit, as shown in Figure 6. A spatially localised structure is present inside the bend, on the outer wall, in the same region where backflow occurs. Looking at the isosurfaces of the spanwise velocity component in Figure 7, it can be noted that this structure is generated at the outer wall of the bend, it moves towards the inner wall as the angular distance inside the bend increases, and then develops in a larger structure downstream of the bend.

The structure of the unstable adjoint eigenmode is also analysed and the pseudocolours of its spanwise velocity component are shown in Figure 8. Significant values are attained in the section upstream of the bend and in that immediately downstream of the bend inlet. These regions are therefore identified with the most receptive to momentum forcing and initial conditions (Giannetti & Luchini, 2007). The large spatial separation between the direct and adjoint eigenmode is an indicator of the non-normality of the linearised Navier–Stokes operator (Chomaz, 2005).

STRUCTURAL SENSITIVITY ANALYSIS

Because of this large spatial separation between the direct and adjoint eigenmode, it is not possible to draw any conclusion about the location of the core of the instability by studying the two modes separately. Therefore, an analysis of the structural sensitivity of the unstable eigenmode to spatially localised velocity feedbacks is performed in order

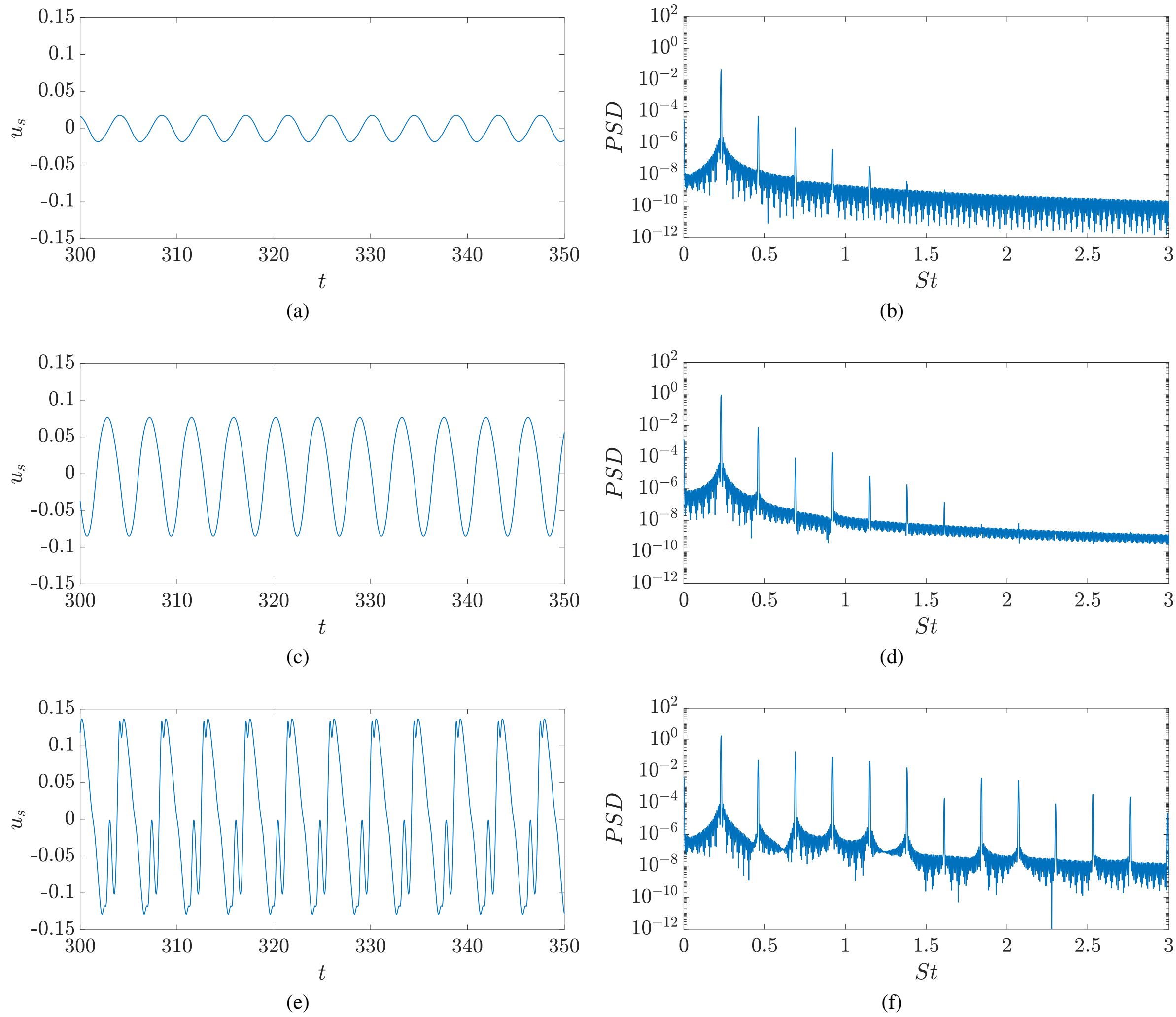

Figure 4: Time signal of the streamwise velocity component for $Re_b = 2550$ and related power spectral density, measured at (a)–(b) $\theta = 30°$, (c)–(d) $s/D = 0$, (e)–(f) $s/D = 4$. The velocity probe is located at $(p, y) = (1.2, -0.3)$ in the cross-section. The Strouhal number is defined as $St = fD/U_b$.

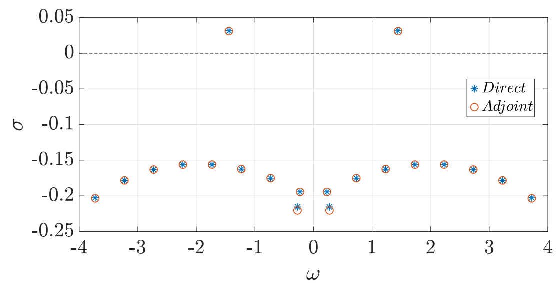

Figure 5: Spectrum for the direct ($*$) and adjoint ($\circ$) problem for $Re_b = 2550$. A pair of unstable complex conjugate eigenvalues $\lambda = 0.0316 \pm i\,1.4402$ is found.

to locate the *wavemaker* (Giannetti & Luchini, 2007). The spatial distribution of the structural sensitivity function η, defined as

$$\eta(\boldsymbol{x}) = \frac{||\hat{\boldsymbol{u}}^{\dagger}(\boldsymbol{x})||\;||\hat{\boldsymbol{u}}(\boldsymbol{x})||}{\int_{\Omega} \hat{\boldsymbol{u}}^{\dagger}(\boldsymbol{x}) \cdot \hat{\boldsymbol{u}}(\boldsymbol{x})\, \mathrm{d}\Omega}, \tag{4}$$

where $\hat{\boldsymbol{u}}(\boldsymbol{x})$ and $\hat{\boldsymbol{u}}^{\dagger}(\boldsymbol{x})$ are the direct and adjoint velocity fields, respectively, is analysed. Significant values are found only in the region inside the bend, on the outer wall, at an angular distance of approximately 15° from the bend inlet, as can be observed in Figure 9. Since this is a region of backflow, it is concluded that a shear layer instability occurs, with a feedback mechanism generated by the recirculation.

CONCLUSIONS

The laminar and transitional flow in a 90°-bend pipe is investigated by means of direct numerical simulations. It is found that the flow is steady for $Re_b \leq 2500$ and it turns unsteady when the Reynolds number is increased. It is observed that a purely periodic regime is well established at $Re_b = 2550$. A global stability analysis is performed in order to study the origin of the transition from the steady to the periodic regime. A pair of unstable complex conjugate eigenvalues, with a frequency very close to that measured in DNS, is found. It is then concluded that the flow is globally unstable for $Re_b \gtrapprox 2529$ due to a Hopf bifurcation. This value is significantly lower than for the corresponding flow in a torus.

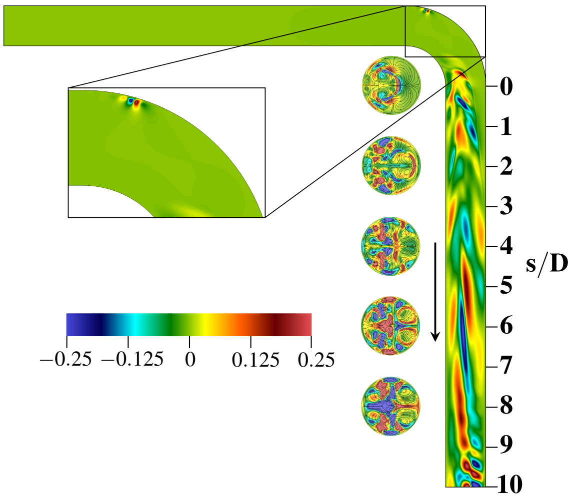

Figure 6: Real part of the unstable eigenmode for $Re_b = 2550$. In the symmetry plane pseudocolours of the spanwise velocity component u_p are shown, whereas the cross-sections show in-plane streamlines and pseudocolours of the streamwise velocity component u_s. Arbitrary units. The arrow indicates the flow direction. *Inset:* magnified view of the structure present inside the bend.

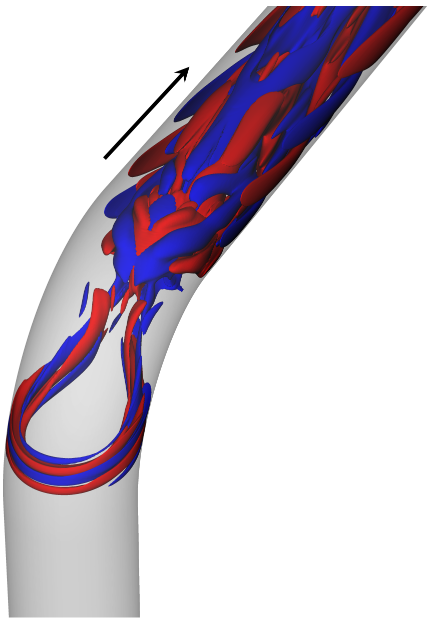

Figure 7: Isosurfaces of the spanwise velocity component u_p of the real part of the unstable eigenmode in the bend region for $Re_b = 2550$. Values in the range $[-0.25, 0.25]$ are shown. Red surfaces indicate positive values, whereas blue surfaces represent negative ones. Arbitrary units. The arrow indicates the flow direction. Alternation of positive and negative values is observed at the outer wall of the bend.

The investigation of the spatial structure of both the direct and adjoint unstable eigenmodes shows a large spatial separation between the two, making it impossible to draw conclusions about the origin of the instability by analysing the

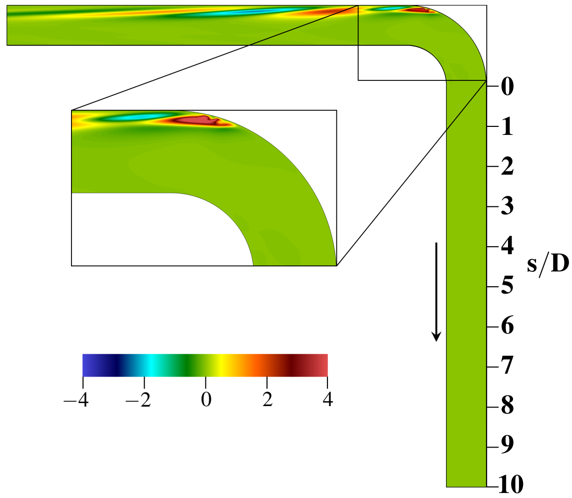

Figure 8: Real part of the unstable adjoint mode for $Re_b = 2550$. The pseudocolours of the spanwise velocity component u_p in the symmetry plane are shown. Arbitrary units. The arrow indicates the flow direction. *Inset:* magnified view of the bend region. A large receptivity to momentum forcing and initial conditions is observed in the inlet section and in the region just after the bend inlet, on the outer wall.

two modes separately. To this end, an analysis of the structural sensitivity of the unstable eigenmode to spatially localised feedbacks is performed. It is found that the structural sensitivity function η exhibits significant values inside the bend, on the outer wall, approximately 15° downstream of the bend inlet. Since in this region backflow occurs, the instability is a shear layer one. The influence of the curvature ratio on the stability properties of the flow has to be further understood, for the purpose of tracing a complete bifurcation diagram.

ACKNOWLEDGEMENTS

This study was funded by the Swedish Research Council (VR). The simulations were performed on resources provided by the Swedish National Infrastructure for Computing (SNIC) at PDC (KTH Stockholm) and NSC (Linköping University).

REFERENCES

Bagheri, S., Åkervik, E., Brandt, L. & Henningson, D. S. 2009 Matrix-free methods for the stability and control of boundary layers. *AIAA Journal* **47** (5), 1057–1068.

Berger, S. A., Talbot, L. & Yao, L. S. 1983 Flow in curved pipes. *Annual Review of Fluid Mechanics* **15** (1), 461–512.

Canton, J., Örlü, R. & Schlatter, P. 2017 Characterisation of the steady, laminar incompressible flow in toroidal pipes covering the entire curvature range. *International Journal of Heat and Fluid Flow* **66**, 95–107.

Canton, J., Rinaldi, E., Örlü, R. & Schlatter, P. 2019 A critical point for bifurcation cascades and featureless turbulence, arXiv:1904.13314v2 .

Canton, J., Schlatter, P. & Örlü, R. 2016 Modal instability

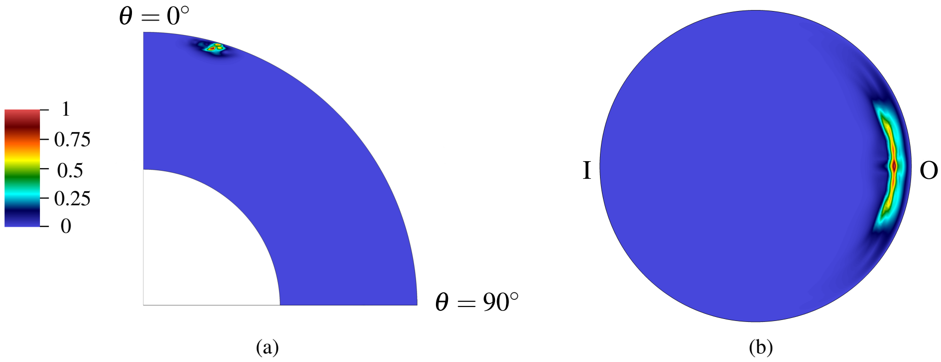

Figure 9: Pseudocolours of the structural sensitivity function of the unstable mode (a) in the symmetry plane and (b) in the cross-section at $\theta = 15^\circ$. Values are normalised with respect to the maximum. The line connecting I and O represents the inner-outer plane.

of the flow in a toroidal pipe. *Journal of Fluid Mechanics* **792**, 894–909.

Chomaz, Jean-Marc 2005 Global instabilities in spatially developing flows: non-normality and nonlinearity. *Annual Review of Fluid Mechanics* **37** (1), 357–392.

Citro, V., Luchini, P., Giannetti, F. & Auteri, F. 2017 Efficient stabilization and acceleration of numerical simulation of fluid flows by residual recombination. *Journal of Computational Physics* **344**, 234–246.

Dean, W. R. 1927 XVI. Note on the motion of fluid in a curved pipe. *The London, Edinburgh, and Dublin Philosophical Magazine and Journal of Science* **4** (20), 208–223.

Fischer, P. F., Lottes, J. W. & Kerkemeier, S. G. 2008 nek5000 web page, http://nek5000.mcs.anl.gov.

Giannetti, F. & Luchini, P. 2007 Structural sensitivity of the first instability of the cylinder wake. *Journal of Fluid Mechanics* **581**, 167–197.

Kühnen, J., Braunshier, P., Schwegel, M., Kuhlmann, H. C. & Hof, B. 2015 Subcritical versus supercritical transition to turbulence in curved pipes. *Journal of Fluid Mechanics* **770**, R3.

Kühnen, J., Holzner, M., Hof, B. & Kuhlmann, H. C. 2014 Experimental investigation of transitional flow in a toroidal pipe. *Journal of Fluid Mechanics* **738**, 463–491.

Lehoucq, R. B., Sorensen, D. C. & Yang, C. 1998 *ARPACK Users' Guide: Solution of Large-Scale Eigenvalue Problems with Implicitly Restarted Arnoldi Methods*. Society for Industrial and Applied Mathematics.

Nandakumar, K. & Masliyah, J. H. 1982 Bifurcation in steady laminar flow through curved tubes. *Journal of Fluid Mechanics* **119**, 475–490.

Peplinski, A., Schlatter, P. & Henningson, D. S. 2015 Global stability and optimal perturbation for a jet in cross-flow. *European Journal of Mechanics - B/Fluids* **49** (Part B), 438–447.

Rinaldi, E., Canton, J. & Schlatter, P. 2019 The vanishing of strong turbulent fronts in bent pipes. *Journal of Fluid Mechanics* **866**, 487–502.

Schlatter, P., Bagheri, S. & Henningson, D. S 2011 Self-sustained global oscillations in a jet in crossflow. *Theoretical and Computational Fluid Dynamics* **25** (1), 129–146.

Sorensen, D. C. 1992 Implicit application of polynomial filters in a k-step Arnoldi method. *SIAM Journal on Matrix Analysis and Applications* **13** (1), 357–385.

Tunstall, R., Laurence, D., Prosser, R. & Skillen, A. 2016 Large eddy simulation of a T-Junction with upstream elbow: the role of Dean vortices in thermal fatigue. *Applied Thermal Engineering* **107**, 672–680.

Vashisth, S., Kumar, V. & Nigam, K. D. P. 2008 A review on the potential applications of curved geometries in process industry. *Industrial & Engineering Chemistry Research* **47** (10), 3291–3337.

Yamano, H., Tanaka, M., Murakami, T., Iwamoto, Y., Yuki, K., Sago, H. & Hayakawa, S. 2011 Unsteady elbow pipe flow to develop a flow-induced vibration evaluation methodology for Japan sodium-cooled fast reactor. *Journal of Nuclear Science and Technology* **48** (4), 677–687.